Electromagnetic dissociation of ^{28}Si at $E_{lab}/A = 14.6$ GeV by nucleon emission

J. Barrette,[a] P. Braun-Munzinger,[b] W. E. Cleland,[c] G. David,[b] E. Duek,[d] M. Fatyga,[d] D. Fox,[e] S. V. Greene,[f] J. R. Hall,[g] R. Heifetz,[h] T. K. Hemmick,[f] N. Herrmann,[b,*] R. W. Hogue,[d] G. Ingold,[b] K. Jayananda,[c] D. Kraus,[c] A. Legault,[a] D. Lissauer,[d] W. J. Llope,[b] T. Ludlam,[d] R. Majka,[f] D. Makowiecki,[d] S. K. Mark,[a] J. T. Mitchell,[f] M. Muthuswamy,[b] E. O'Brien,[d] L. H. Olsen,[d,*] V. Polychronakos,[d] M. Rawool-Sullivan,[e] F. S. Rotondo,[f] J. Sandweiss,[f] B. Shivakumar,[f] J. Simon,[i] U. Sonnadara,[c] J. Stachel,[b] J. Sunier,[e] H. Takai,[d] T. G. Throwe,[d] H. VanHecke,[e] L. Waters,[b] W. J. Willis,[j] K. Wolf,[i] D. Wolfe,[g] and C. L. Woody[d]

[a]*McGill University, Montreal, Canada*
[b]*State University of New York, Stony Brook, Stony Brook, New York 11794*
[c]*University of Pittsburgh, Pittsburgh, Pennsylvania 15260*
[d]*Brookhaven National Laboratory, Upton, New York 11973*
[e]*Los Alamos National Laboratory, Los Alamos, New Mexico 87545*
[f]*Yale University, New Haven, Connecticut 06511*
[g]*University of New Mexico, Albuquerque, New Mexico 87131*
[h]*University of Tel Aviv, Tel Aviv, Israel*
[i]*Texas A&M University, College Station, Texas 77843*
[j]*CERN, Geneva, Switzerland*

(E814 Collaboration)

(Received 20 November 1989)

Electromagnetic dissociation cross sections for one, two, and three nucleon removal were measured for an $E_{lab}/A = 14.6$ GeV ^{28}Si beam impinging on ^{27}Al, ^{120}Sn, and ^{208}Pb targets. The measured cross sections exhibit an approximate Z_T^2 dependence and are well reproduced by calculations convoluting the virtual photon spectrum with the experimental $\sigma(\gamma,N)$ photonuclear cross sections. Comparison with other experimental results and energy dependence of the cross sections are discussed.

I. INTRODUCTION

The acceleration of heavy ions in the Alternating Gradient Synchrotron (AGS) facility at Brookhaven National Laboratory (BNL) and the Super Proton Synchrotron (SPS) at European Organization for Nuclear Research (CERN) makes the study of nuclear collisions at relativistic energies possible. The high bombarding energies open up a unique opportunity to study the different aspects of reaction mechanisms at large impact parameters. In such collisions the projectile is subject to excitation by a short electromagnetic pulse provided by the electric charge of the target and enhanced by the Lorentz contraction (see Ref. 1 and references quoted therein). The fragmentation process at large impact parameters can be produced by either the nuclear or the Coulomb field of the target nucleus. Since the two processes can give rise to the same final state, they cannot be distinguished in a given event. Their cross sections can, however, be differentiated by their dependence on target charge (or mass).

In a pure electromagnetic dissociation process the projectile is excited by the electromagnetic field and subsequently decays by means of hadronic fragmentation or gamma ray emission. An alternative description of the reaction process can be made by replacing the target electromagnetic field with an equivalent virtual photon flux. In such a picture the projectile is excited by the absorption of a virtual photon followed by a dissociation similar to a real (γ,N) photonuclear reaction. While different excitation modes of the projectile are dictated by its nuclear properties, the virtual photon spectrum can be obtained for calculation purposes from classical electrodynamics, e.g., by the Weizsäcker-Williams formulation.[2] This flux as seen by the projectile is proportional to the square of the target charge number Z_T. Because of the low photon momenta involved, the nuclear form factor is assumed to be unity. The cross section for projectile dissociation into a specific channel ξ is given by the following expression:

$$\sigma(\xi) = \int_0^{E_{\max}} N_\gamma \sigma(\gamma,\xi) dE_\gamma \ , \tag{1.1}$$

where N_γ is the virtual photon flux already integrated over all impact parameters, $\sigma(\gamma,\xi)$ is the measured cross section for the photonuclear reaction into the channel in question, and $E_{\max}$ is the maximum virtual photon energy.

In Fig. 1 we show the virtual photon spectra expected at different beam momenta for ^{28}Si impinging on a ^{208}Pb target. The photon spectrum hardens with increasing in-

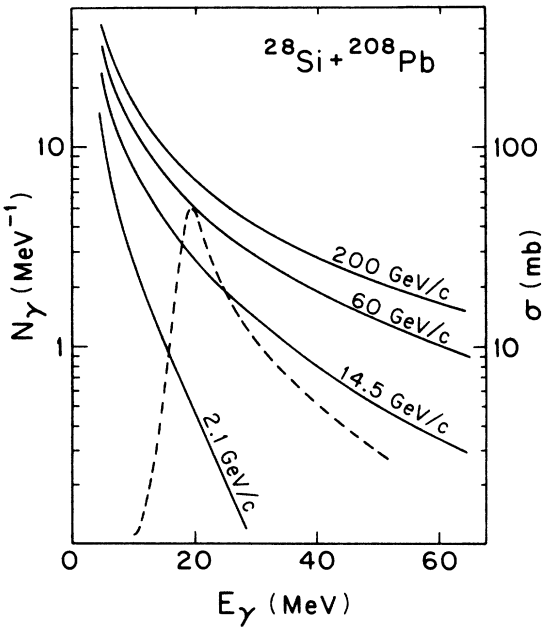

FIG. 1. Virtual photon spectrum for ^{28}Si + ^{208}Pb for different beam momenta (left-hand scale) superimposed on the cross section (right-hand scale) for real photon absorption by the ^{28}Si nucleus.

cident momentum, due to the increasing Lorentz contraction of the field as seen by the projectile. The dashed line represents the experimental cross section for total photon absorption by the projectile,[3] which is dominated by its Giant Dipole Resonance (GDR). The relatively large overlap between the photon flux and the GDR absorption curve permits selective excitation of the GDR and hence makes possible the study of rare resonance decay modes. Furthermore, the high flux of photons enhances the probability of multiphoton absorption by the projectile. This could lead to multiple excitation of the isovector giant dipole resonance, thereby producing a relatively cold separation of neutrons and protons in the projectile.[1,4]

In this paper we report the cross section for the electromagnetic excitation of the ^{28}Si nucleus in the region of the GDR, followed by decay into a variety of final states, and its dependence on target charge. This is the first measurement of the Electromagnetic Dissociation (EMD) into exclusive channels at relativistic energies where all residual fragments are detected and identified. The cross sections were measured in the E814 experimental setup, described in Sec. II, by selecting peripheral collisions through the identification of all final-state fragments and the rejection of events that induce target excitation or secondary particle production. The singular capabilities of the E814 apparatus provide a powerful way to reject peripheral interactions initiated by the nuclear field. Details of our analysis and data reduction are presented in Sec. III. A discussion of our results and comparisons to previous measurements[5–12] at different energies is presented in Sec. IV.

II. EXPERIMENTAL SETUP

The E814 experimental setup is shown in Fig. 2. For the purpose of this discussion, we divide the detectors into two groups, each serving a specific function. The upstream set of detectors, consisting of the target calorimeter, target scintillators, participant calorimeter, and the silicon multiplicity detector, are designed to detect reaction products and target fragments at large angles, such as those produced in more central collisions. The downstream set of detectors are the drift chambers, uranium calorimeters, forward scintillators and magnet scintillators, which together form the forward spectrometer. The spectrometer is used to determine the momentum of those charged particles passing through a ± 12.3 mrad vertical by ± 18.4 mrad horizontal aperture defined by the participant calorimeter.

A set of scintillators comprising the beam telescope is

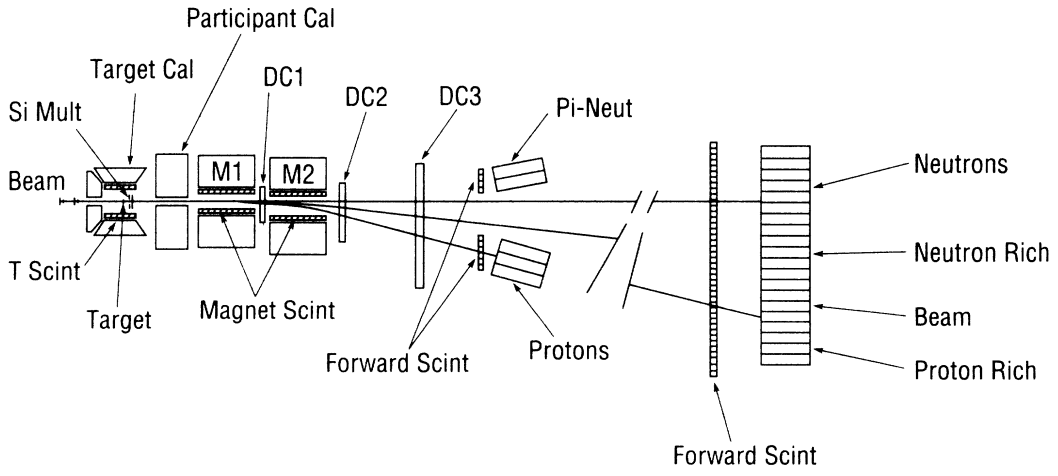

FIG. 2. E814 experimental setup. M1 and M2 are dipole magnets. DC1, DC2, and DC3 are drift chambers used to track particles in the forward spectrometer. Solid lines in the figure represent trajectories for neutral particles, beamlike particles (with $Z/A = \frac{1}{2}$) and protons with 14.6 GeV/c momentum.

used to define acceptable beam particles. The telescope is designed to ensure the presence of a single beam particle with the ionization of a ^{28}Si nucleus. It, together with the beam optics, defines a beam spot on the target of approximately 10.0 mm^2. The target is mounted inside the target calorimeter.

Interaction products emitted at angles greater than 45° with respect to the beam direction are detected in the target calorimeter and target scintillators. The target calorimeter is an assembly of 992 NaI crystals. The crystals, each 13.8-cm deep (5.3 radiation lengths), face the target and are mounted in five separate boxes. The four side walls are located around the target and parallel to the beam trajectory covering $45° < \theta < 118°$, while the back wall covers the angular range $135° < \theta < 165°$. The target scintillators consist of 52 strips of plastic scintillator covering the inner four side walls of the target calorimeter. Reaction products emerging in the angular range 2.0–33.5° are detected by the silicon multiplicity detector. The coverage of the participant calorimeter, not used in this analysis, extends from 2° to 45°. The multiplicity detector is composed of two concentric silicon discs, each 300-μm thick and segmented into 512 pads. The upstream disc has an angular coverage from 15.8° to 33.5°, and the downstream disc covers from 2.0° to 19.0°. The total number of hits and the hit pattern are recorded for each event.

The forward spectrometer is located downstream of the participant calorimeter. The spectrometer is composed of tracking chambers (DC1, DC2, and DC3), uranium calorimeters, dipole magnets (M1 and M2), and an array of plastic scintillators. The forward spectrometer permits the determination of the charge, momentum, and energy of the reaction products. The uranium calorimeters are described in detail elsewhere.[13] The modules are distributed in groups and labeled according to those trajectories followed by reaction fragments emitted at 0° with beam rapidity. The forward scintillation counters, each of dimensions $10.0 \times 1.0 \times 120.0$ cm^3 are located in front of the calorimeters. Since they are half of the width of the calorimeter cells, two counters are associated with each calorimeter unit. The distance from the furthest downstream forward scintillators to the target is approximately 31 m. Thus coarse Z/A information for particles with beam rapidity is obtained by the position of the hit in the forward scintillator array. Scintillators are also mounted inside the dipole magnets and are primarily designed to detect pions produced in grazing collisions. This array consists of 16 scintillators distributed equally between the first and second dipole magnets. Helium bags occupy the two largest vacant regions between the detectors in the forward spectrometer, and serve to minimize secondary interactions.

The data presented in this paper were measured without the use of the participant calorimeter and tracking detectors since at that time they were only partially instrumented. However, the information obtained from the other detectors is complete enough to identify both heavy and light products from peripheral fragmentation.

The requirement that light products ($1p$, $1n$, $2p$, $2n$, etc.) be detected simultaneously with a heavy fragment was used as an event trigger for the data acquisition. A heavy fragment was defined as a projectile-like fragment with charge number $Z \geq 10$ detected in any of the forward scintillators near the path of the beam projectiles. A typical resolution of 3% in pulse height was obtained for the forward scintillators. Protons or neutrons were identified by measurement of the energy deposited in the appropriate calorimeters. The signals from calorimeter modules in the neutron and proton regions were added to provide the total energy information for the trigger. Since the resolution of the total energy measurement is approximately 10% for $E_{\rm lab} = 14.6$-GeV nucleons, the association of the number of nucleons with deposited energy peaks is unambiguous. Furthermore, it was required that for $1n$ or $1p$ events the energy deposition be contained within two adjacent calorimeter modules, so that background events that deposit little energy per module but substantial total energy were rejected.

All the operations described above were performed at the trigger level for which digitized values of analog trigger sums were used. The trigger system was designed to allow data taking with parallel triggers with the possibility of accepting a small fraction of the high rate triggers, thus enhancing the number of rare events in a given data sample. In this work, events with decays by single nucleon emission were reduced relative to those with decays via multinucleon emission. Upon the generation of a trigger, digitized signals from all detectors were written to magnetic tape for later off-line reconstruction. Beam particles as defined by the beam telescope were scaled for normalization purposes.

The three targets used were ^{27}Al, ^{120}Sn, and ^{208}Pb. Each was isotopically enriched to 99.99%. The target thicknesses were 4.36, 3.25, and 1.30 g/cm^2, respectively. In addition, data with an empty target holder were taken to evaluate residual interactions with beam scintillators and materials surrounding the target. Events requiring only the presence of a beam particle were interleaved with the normal data to help evaluate the efficiency of the cuts applied in the selection of events and the probability of downstream interactions. Two sets of data were taken. In the first set, triggers for either protons or neutrons in the final state were run in parallel. In the second part of the run, only data in which neutrons were detected were taken in order to enhance the statistics for these events.

III. DATA REDUCTION AND RESULTS

The events accumulated on tape are further processed by correcting the data from the scintillators and calorimeters and through the imposition of selection criteria. To enhance EMD processes, we select events in which no particles apart from the beam fragments are produced and the target is left mostly intact. Two types of cross sections are obtained. The first kind of cross section, designated semi-inclusive, is for channels decaying by xn or yp emission ($x,y = 0,1,2\ldots$) with no additional requirement on the Z of the accompanying heavy fragment. Since a threshold on Z of the heavy fragment was imposed at the trigger level, truly inclusive cross sections cannot be obtained. The second type of cross section is

for exclusive channels, where the complete final residues are identified. Cross sections are measured for the following reactions on ^{27}Al, ^{120}Sn, and ^{208}Pb targets: (1) $^{28}\text{Si}\rightarrow xn+$heavy fragment, $x=1,2$ (semi-inclusive), (2) $^{28}\text{Si}\rightarrow yp+$heavy fragment, $y=1,2,3$ (semi-inclusive), (3) $^{28}\text{Si}\rightarrow 1n+^{27}\text{Si}$, (4) $^{28}\text{Si}\rightarrow 1p+^{27}\text{Al}$, (5) $^{28}\text{Si}\rightarrow 2n+^{26}\text{Si}$, (6) $^{28}\text{Si}\rightarrow 2p+^{26}\text{Mg}$, (7) $^{28}\text{Si}\rightarrow 1n\,1p+^{26}\text{Al}$, (8) $^{28}\text{Si}\rightarrow 2p\,1n+^{25}\text{Mg}$, (9) $^{28}\text{Si}\rightarrow 2n\,1p+^{25}\text{Al}$, and (10) $^{28}\text{Si}\rightarrow 2n\,2p+^{24}\text{Mg}$.

The preceding reactions are expected to be produced predominantly via electromagnetic dissociation. However, there is a non-negligible contribution arising from strong interactions, which is an important fraction of events for low-Z targets. The hadronic component of the cross section is expected to scale with the radius of the target, whereas the electromagnetic component is expected to scale with the square of target charge number, modified only by the target and beam form factors. The background to the preceding reactions comes mostly from instances where additional pions are produced in the final state. These events are eliminated by rejecting events in which there were signals in the detectors surrounding the target or in the magnet scintillators. To filter the events even further we carry out a cluster analysis,[13] which locates individual hadronic showers and partitions the energy accordingly. This permits a determination of the number of neutrons and protons for a given event by associating them with clusters of the appropriate energy. The forward scintillators give us a measurement of the Z of the forward fragments. For the exclusive reactions we demand that the Z value found from the pulse height in the forward scintillator agrees with the fragment charge number Z for the channel in question.

The information used to reject background events is the following.

Target scintillators. The pulse height from each of the target scintillators was discriminated at minimum ionizing level and at four times the minimum ionizing level. The higher threshold discriminators count heavily ionizing target fragments, while the lower threshold units count all charged particles produced in the collision as well as delta rays that accompany the beam. Cuts are made in these counters to eliminate target breakup or evidence of large multiplicity in the target region. A multiplicity of five and three hits are required for the lower and higher thresholds, respectively.

Target calorimeter. The target calorimeter is sensitive to charged hadrons and electrons or photons in the angular region $\theta\geq 45°$. We require that there is no energy deposit greater than 15 MeV in any one of the 992 crystals.

Multiplicity counter. The multiplicity counter is sensitive to charged particle tracks emitted in the forward cone, including delta rays from the target. Therefore, only events with a multiplicity of twenty or greater are removed from the sample.

Magnet scintillators. The magnet scintillators are sensitive to slow charged particles deflected inside the dipole magnets. We require a multiplicity of three as a minimum condition for rejecting an event.

Forward scintillators. The signals from the forward scintillators are corrected for beam rate dependence, and gain corrections were determined from the peaks in the spectrum corresponding to different Z fragments.

Forward calorimeter. A cluster-finding algorithm[13] is used to reject events that are generated by sparse deposition of energy or electronically induced noise. For a given final state, e.g., $1p+^{27}\text{Al}$ or $1n+^{27}\text{Si}$, we require the number of neutrons and/or proton clusters to be consistent with the final state assignment.

In Fig. 3 we show the cross sections for reactions 1 and 2, for the three targets. Error bars in this figure indicate only statistical uncertainties. The cross sections are corrected for efficiency of selection criteria and for the contribution of downstream interactions. The largest uncertainty in the measurement of the cross section is the rejection efficiency for quasiperipheral processes, where one or more pions are produced. This background is more important for low-Z targets, for which the ratio of the Coulomb dissociation to the total hadronic cross section is small. We estimate the systematic error in the measurement to be approximately 20% for ^{27}Al target and 5% for ^{208}Pb target. The cross sections for heavy targets exhibit a Z_T^{α} dependence, with $\alpha\approx 1.8$. The ratio between $1n$ and $1p$ semi-inclusive cross sections is 2.5 ± 0.3 for the ^{208}Pb target. The value of this ratio observed in $^{28}\text{Si}(\gamma,p)$ and $^{28}\text{Si}(\gamma,n)$ photonuclear reactions[3] is in agreement with our measurements. The solid and

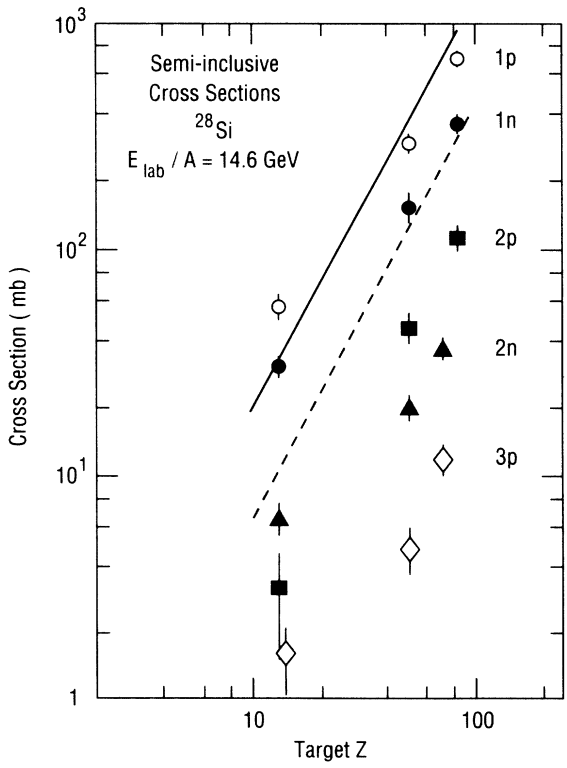

FIG. 3. Semi-inclusive cross sections for few nucleon removal from ^{28}Si. The error bars indicate statistical uncertainties. The solid line and the dashed line represent results from calculations where the virtual photon spectrum is folded with experimental $\sigma(\gamma,p)$ and $\sigma(\gamma,n)$ cross sections, respectively.

dashed lines are results of calculations based on Eq. (1.1). For each target, the virtual photon spectrum is generated and convoluted with the experimental photonuclear cross sections. The discrepancies between calculated and measured cross section for ^{27}Al is very likely due to the remaining hadronic component at the lowest Z_T. The Z_T dependence and the absolute scale of the cross section for ^{208}Pb and ^{120}Sn are in good agreement with the calculation.

In Fig. 4, cross sections are shown for the same reactions, but for those events that produce signals in the detectors surrounding the target. As indicated in the figure, the cross sections for those events appear to be proportional to $A_T^{1/3}$, in which A_T is the target mass, as expected for mechanisms which in a geometrical picture require contact at the periphery of the target nucleus. These events are expected to be dominated by hadronic processes. Note that the ratio of $1p$ to $1n$ cross sections is 1.5 ± 0.3, which is close to unity and suggests a similar production mechanism. The dashed line in Fig. 4 represents results from calculations based on the limiting fragmentation model with parameters from Brechtmann *et al.*[8] for the removal of one charge unit. The solid line in Fig. 4 represents results from a geometrical calculation as suggested by Benesh *et al.*[14] In this model it is assumed that the contribution to the single nucleon removal cross section comes from an annular region 0.5-fm wide around the target nucleus. Both models describe satisfactorily the measured cross sections and reinforce the conclusion that the events are produced hadronically.

In Fig. 5 we show cross sections for exclusive reactions 3–10 for all the targets. The error bars indicate statistical uncertainties only. Corrections similar to those used for the semi-inclusive reactions are applied to these cross sections. The systematic errors are again target dependent and estimated to be 15% for ^{27}Al and 5% for ^{208}Pb. The dependence of the cross sections on the target charge number Z_T for the removal of a single nucleon follows closely the $Z_T^{1.8}$ power law as observed in previous studies.[9,10] For the removal of a larger number of nucleons the relative importance of the nuclear component is expected to increase, becoming dominant at low Z_T. At higher Z_T, the contribution from multiple photon exchange may set in and thus we do not necessarily expect a simple power-law dependence. The cross section for the $1p+^{27}$Al channel is two orders of magnitude higher than that for the $2n2p+^{24}$Mg channel. The lines shown in Fig. 5 represents the same calculations as those indicated in Fig. 3, and they also show the expected Z_T dependence for the $1p$ and $1n$ removal channels. Note that the calculations are for inclusive reactions, whereas the cross sections are for exclusive channels. Therefore we expect the experimental results to fall slightly below the calculated values.

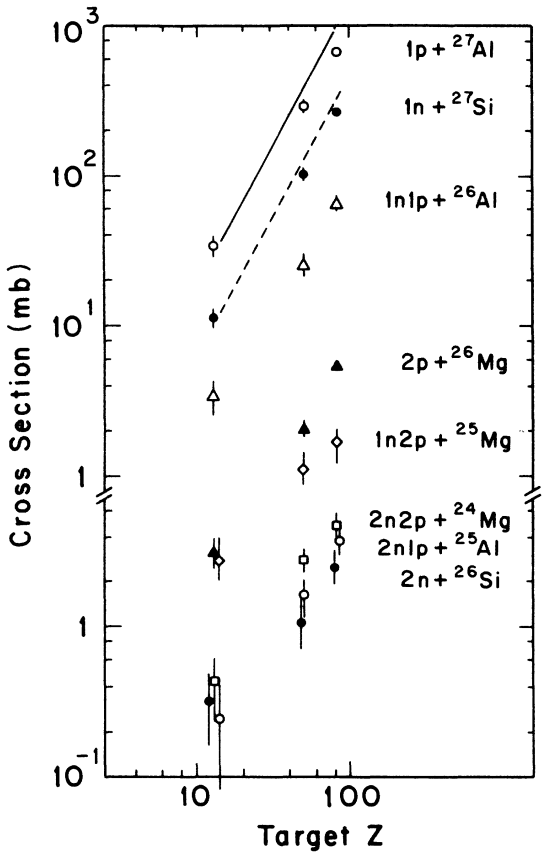

FIG. 5. Exclusive cross sections for seven different channels as function of target charge. Error bars indicate statistical uncertainties.

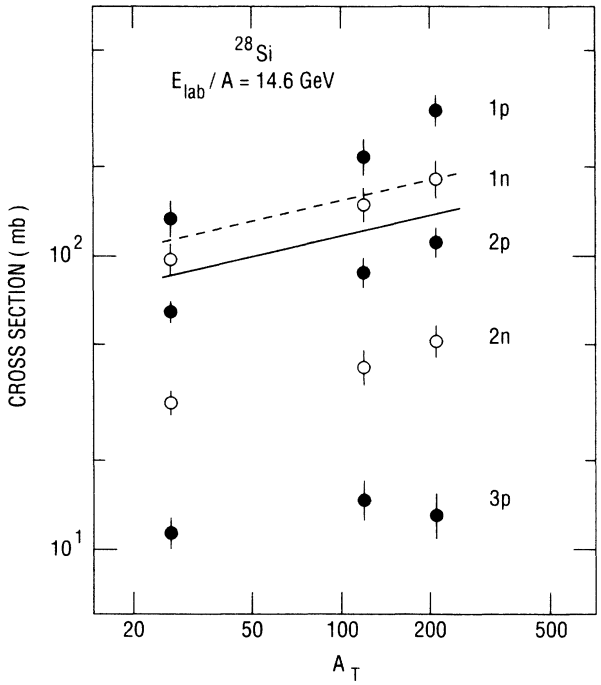

FIG. 4. Semi-inclusive hadronic cross sections for few nucleon removal from ^{28}Si. The dashed line represents results from the limiting fragmentation model from Ref. 8. The solid line represents results from the geometrical model from Ref. 14.

IV. DISCUSSION AND CONCLUSION

In Figs. 3 and 5 we compare the measured cross sections to calculations in which the virtual photon spec-

trum is folded with experimental photonuclear cross sections. Measured cross sections for ^{28}Si(γ,n) and ^{28}Si(γ,p) are available up to $E_\gamma = 30$ MeV and are obtained from Refs. 3, 15, 16, and 17, respectively. The virtual photon spectrum is obtained using the Weizsäcker-Williams method.[2] In evaluating the spectrum one must specify the minimum impact parameter, $b_{\min}$, which affects the shape and the cutoff energy. To check the sensitivity of the calculated cross sections we assume the minimum impact parameter to be

$$b_{\min} = r_0(A_P^{1/3} + A_T^{1/3}) \tag{4.1}$$

and vary r_0 from 1.0 to 1.5 fm. Despite the large variation about the assumed value of 1.2 fm, the variation in absolute value of the cross section is only 30%. These variations in r_0 do not affect significantly the Z_T dependence of the calculated cross sections.

The observed dependence of the measured cross sections on the target charge number Z_T indicates the electromagnetic nature of the excitation. The data for $1p$ and $1n$ channels are in good agreement with the calculated values considering the above-mentioned uncertainties. The differences between the cross sections for $1n$ and $1p$ channels are understood as originating from the decay of the GDR in ^{28}Si. The measured ratio[3] $\sigma(\gamma,p)/\sigma(\gamma,n)$ is 2.7 ± 0.7, for E_γ up to 30 MeV. Our similar value for the cross sections for reactions 1 and 2 is indicative of preferential excitation of the GDR in this experiment. Note that in Fig. 4, where cross sections for hadronic processes events are displayed, this ratio is closer to unity.

While for the high-Z target the electromagnetic process dominates over hadronic processes, the situation is reversed for the lower-Z target. As can be seen from Figs. 3 and 4, the ratio of electromagnetic to hadronic components ranges from 0.4 to 2.5 as the target Z increases from $Z=13$ to $Z=82$ for the $1p$ decay channel.

Our EMD cross sections are displayed in Fig. 6 as function of the Q value for the decay channel where the cross sections are now grouped by target. The exclusive $1p$ and $1n$ channels exhaust 92% and 70% of the semi-inclusive cross sections, respectively. The three channels that decay by two nucleon emission are $1n\,1p$ ($Q=-24.6$ MeV), $2p$ ($Q=-19.9$ MeV), and $2n$ ($Q=-30.5$ MeV). Although the Q value for the $2p+^{26}$Mg channel is lower than that for the $1n\,1p+^{26}$Al channel, the cross section is higher. For all targets the general trend of the data an exponential decrease. It is interesting to note the difference in cross sections between xn channels and yp channels, especially the large difference between $2n+^{26}$Si and $2p+^{26}$Mg channels.

The relative cross sections of the different final states can be understood as due to the decay of the excited projectile. The decay modes of an excited ^{28}Si nucleus were investigated in the GDR region.[17,18] Both the statistical and the nonstatistical nature of the decay have been studied. For the decay via $1p$ emission to individual excited levels in ^{27}Al a large nonstatistical contribution was found, while for alpha emission the data suggests the process is purely statistical.[17] To understand the general trends in Fig. 6, a calculation was performed assuming a statistical decay for the excited ^{28}Si nuclei. Details of this calculation will be reported elsewhere.[19] The excitation energy distribution is obtained by the folding of the virtual photon spectrum and the experimentally known photon absorption cross section. The code CASCADE (Ref. 20) is used to follow the subsequent decay of the ^{28}Si. The results show a good overall agreement with respect to the general trends of the data over the entire range of Q values. In the calculations, level density parameters as implemented in CASCADE and known information on low-lying levels in the relevant residual nuclei were used. On a more detailed level, using such calculations one tends to overestimate the cross sections for channels decaying by proton emission and to underestimate neutron decay cross sections. The largest discrepancy is for the case of $2p$ and $2n$ channels, where the calculations and data differ by a factor of 3. Whether this reflects direct

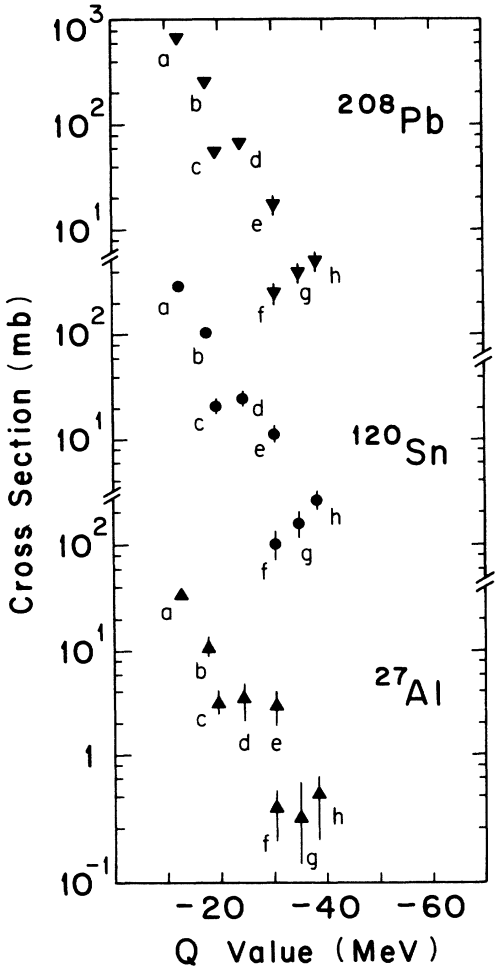

FIG. 6. Cross sections for electromagnetic dissociation as functions of the Q value of the decay channel. Experimental data are grouped according to target type. The label associated with each experimental point indicates a different dissociation channel: (a) $1p+^{27}$Al, (b) $1n+^{27}$Si, (c) $2p+^{26}$Mg, (d) $1n\,1p+^{26}$Al, (e) $2n\,1p+^{25}$Mg, (f) $2n+^{26}$Si, (g) $2n2p+^{24}$Mg, and (h) $2n\,1p+^{25}$Al.

decay mechanisms or is the beginning of a more systematic discrepancy for complex decay channels is an interesting and open question.

Fragmentation of ^{28}Si at $E_{lab}/A = 14.6$ GeV was previously measured by means of plastic nuclear track detectors.[8] In this measurement the inclusive cross sections are determined by detecting only the heavy fragment, thus setting an upper limit for our semi-inclusive measurements. The comparison of our results with those of Brechtmann *et al.*[8] is presented in Fig. 7 as a function of the amount of charge removal. The agreement for $\Delta Z = 1$ is fairly good. Our cross section is lower, as expected, since we do not detect decays via emission of other $Z = 1$ fragments. For $\Delta Z = 2$ the difference is larger but expected, since in our measurement the alpha emission channel is not included. The decay through alpha emission can be as large as 6–10% of the proton emission.[16,17]

The exclusive cross sections obtained in this experiment are larger than those obtained at lower energies and for lighter projectile nuclei, e.g., U(^{18}O,^{17}O) at $E_{lab}/A = 2.1$ GeV.[7] The cross section for this particular channel is 143 mb. The difference is in part due to the stronger excitation of the GDR in this experiment. However, the GDR can be strongly excited at lower energies in heavier nuclei, since $E_{GDR} \sim 80/A^{1/3}$. In fact, the electromagnetic cross section for single neutron emission from ^{197}Au induced by ^{135}La projectiles was measured[5] to be 2.3 b. More recently, measurements of electromagnetic dissociation[21,22] of ^{11}Li induced by several targets were performed at $E_{lab}/A = 0.79$ GeV. A large cross section is indeed observed for the removal of two neutrons. This is attributed to the particular nuclear structure[22] of ^{11}Li. However, the dependence on target charge number Z_T does not show the same power law as observed at higher energies. In general, at lower energies the electromagnetic cross sections show a shallower Z_T dependence in comparison with the higher CERN and AGS bombarding energies.

At CERN energies, $E_{lab}/A = 60$ and 200 GeV, the fragmentation of ^{16}O and ^{32}S has been measured.[9–12] In most cases the total charge-changing cross section is obtained. These cross sections integrate over all residues with charge smaller than that of the projectile. Because of the extremely high-Z resolution in the plastic nuclear track data, the cross section for the removal of several charge units is obtained. The measurements do not determine the removed number of neutrons. In most cases the electromagnetic component is obtained by subtracting the hadronic contribution using estimated values based on the concept of limiting fragmentation. Such an assumption is not made for the cross sections obtained by the NA36 collaboration,[10] where collisions producing secondary particles are electronically rejected. However, again only total charge-changing cross sections as a function of the target charge are obtained. At 200 GeV the ratio of electromagnetic to hadronic cross section for ^{32}S incident on ^{208}Pb is larger than ten, which displays the dominance of electromagnetic over nuclear processes. The excitation of the GDR should not be significantly enhanced over that at AGS energies, although the photon spectrum is harder at higher energies, as is shown in Fig. 1. Since the cutoff value at $E_{lab}/A = 200$ GeV is approximately 4.0 GeV, other excitation modes such as the delta resonance can be excited.

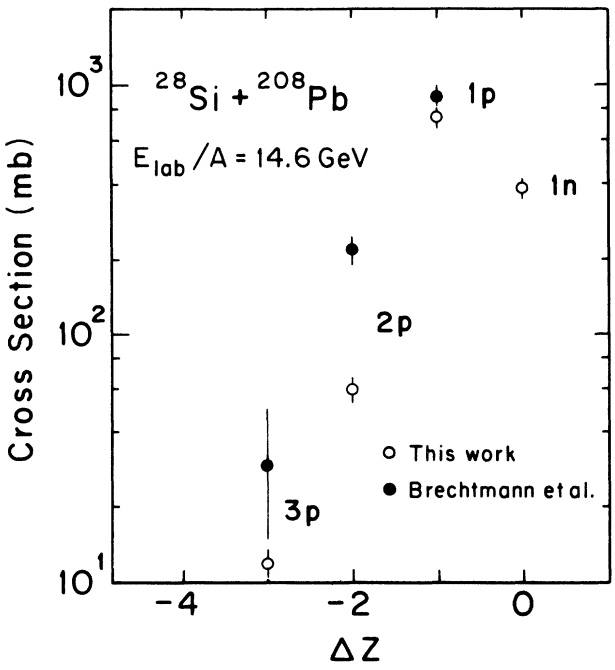

FIG. 7. Semi-inclusive electromagnetic cross sections obtained in this work (blank circles) compared to those from Ref. 8 (solid circles) plotted as function of units of charge removal.

In summary, we have measured the Z_T dependence of EMD cross sections into a number of semi-inclusive and exclusive channels. This first measurement of exclusive cross sections, where all the residual fragments are identified, allows a detailed check of the virtual photon method for the evaluation of electromagnetic cross sections. The experimental cross sections show a $Z_T^{1.8}$ dependence on the target charge number, which is well reproduced by the Weizsäcker-Williams approximation. The target charge dependence is the same as seen at higher energies, but considerably steeper than observed at Bevalac energies. The ability to experimentally separate the sample of events originating from electromagnetic processes from those that induce target excitation or secondary particle production, is of fundamental importance for investigating electromagnetic processes of higher order where hadronic processes become dominant.

ACKNOWLEDGMENTS

We acknowledge the excellent support by the BNL AGS and Tandem staffs and thank Drs. Y. Makdisi and H. Brown for expert help in the design and running of our beam line. This research is supported, in part, by the U.S. Department of Energy, the National Science Foundation, and the Natural Science and Engineering Research Council of Canada.

*Present address: Physikalisches Institut, Universität Heidelberg, Heidelberg, Germany.

[1]P. Braun-Munzinger *et al.*, Proposal E814 submitted to the AGS Program Committee, 1985.

[2]J. D. Jackson, *Classical Electrodynamics* (Wiley, New York, 1975).

[3]R. E. Pywell, B. L. Berman, J. W. Jury J. G. Woodworth, K. G. McNeil, and M. N. Thompson, Phys. Rev. C **27**, 960 (1983).

[4]G. Baur and C. Bertulani, Phys. Rep. **163**, 299 (1988).

[5]J. C. Hill, F. K. Wohn, J. A. Winger, M. Khayat, and K. Leininger, Phys. Rev. C **38**, 1722 (1988).

[6]J. C. Hill, F. K. Wohn, J. A. Winger, M. Khayat, and M. T. Mercier, Phys. Rev. C **39**, 524 (1989).

[7]D. L. Olson, B. L. Berman, D. E. Greiner, H. H. Heckman, P. J. Lindstrom, G. D. Westfall, and H. J. Crawford, Phys. Rev. C **24**, 1529 (1981).

[8]C. Brechtmann, W. Heinrich, and E. V. Benton, Phys. Rev. C **39**, 2222 (1989).

[9]C. Brechtmann and W. Heinrich, Z. Phys. A **330**, 407 (1988).

[10]C. Brechtmann and W. Heinrich, Z. Phys. A **331**, 463 (1988).

[11]P. B. Price, R. Guoxiao, and W. T. William, Phys. Rev. Lett. **61**, 2193 (1988).

[12]E. Anderson *et al.*, CERN Report No. CERN-EP/89-35, 1989.

[13]M. Fatyga, D. Makowiecki, and W. J. Llope, Nucl. Instrum. Methods (in press).

[14]C. J. Benesh, B. C. Cook, and J. P. Vary, Phys. Rev. C **40**, 1198 (1989).

[15]J. T. Caldwell, R. R. Harvey, R. L. Bramblet, and S. C. Fultz, Phys. Lett. **6**, 213 (1963).

[16]A. Veyssiere, H. Beil, R. Bergere, P. Carlos, A. Lepretre, and A. de Miniac, Nucl. Phys. **A227**, 513 (1974).

[17]R. L. Gulbranson, L. S. Cardman, A. Doron, A. Erell, K. R. Lindgren, and A. I. Yavin, Phys. Rev. C **27**, 470 (1983).

[18]E. Kerhove, P. Berkvens, R. van de Vyver, H. Ferdinande, P. van Otten, D. Ryckbosch, and E. Van Camp, Nucl. Phys. **A474**, 387 (1987).

[19]W. J. Llope and P. Braun-Munzinger (unpublished).

[20]F. Pühlhofer, Nucl. Phys. **A280**, 267 (1977).

[21]T. Kobayashi, O. Yamakawa, K. Omata, K. Sugimoto, T. Shimoda, N. Takahashi, and I. Tanihata, Phys. Rev. Lett. **60**, 2599 (1988).

[22]T. Kobayashi *et al.*, KEK Report No. 89-27 (1989).